

# Zero-Shot Low Light Image Enhancement with Diffusion Prior

Joshua Cho    Sara Aghajanzadeh    Zhen Zhu    D. A. Forsyth  
 University of Illinois Urbana-Champaign  
 {joshua66, saraa5, zhenzhu4, daf}@illinois.edu

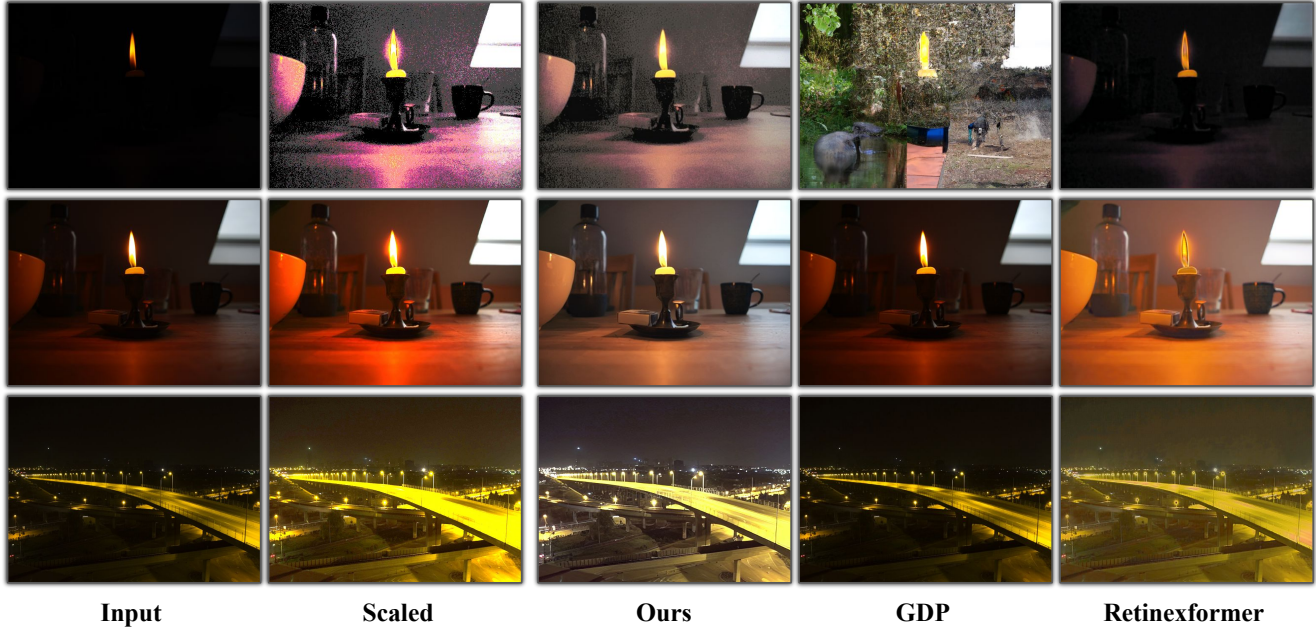


Figure 1. In this paper, we introduce a zero-shot framework for low-light image enhancement that harnesses a large-scale pre-trained diffusion model. While diffusion models, given their enriched knowledge of real image distributions, have shown promising results in image restoration and enhancement tasks, they are liable to *hallucinate* with notably dark, noisy input. In addition, we address the inherent challenges of generalizability in current supervised methods, which are confined by the training data distribution. For example, GDP [9], a recent zero-shot diffusion-based method, hallucinates by introducing non-existent elements (row 1), and Retinexformer, a leading supervised method, exhibits variability in the same candle scene (row 1 and 2) and color shift (row 3), as opposed to our method.

## Abstract

*Balancing aesthetic quality with fidelity when enhancing images from challenging, degraded sources is a core objective in computational photography. In this paper, we address low light image enhancement (LLIE), a task in which dark images often contain limited visible information. Diffusion models, known for their powerful image enhancement capacities, are a natural choice for this problem. However, their deep generative priors can also lead to hallucinations, introducing non-existent elements or substantially altering the visual semantics of the original scene. In this work, we introduce a novel zero-shot method for controlling and refining the generative behavior of diffusion models for dark-to-light image conversion tasks. Our*

*method demonstrates superior performance over existing state-of-the-art methods in the task of low-light image enhancement, as evidenced by both quantitative metrics and qualitative analysis. Code is available [here](#).*

## 1. Introduction

Low-light image enhancement (LLIE) aims to enhance images captured in suboptimal lighting conditions into their natural, well-lit counterpart. Its relevance spans from photography [29] to a wide range of downstream applications such as autonomous driving [27], underwater image enhancement [26, 40], and video surveillance [54]. However, it is a challenging task due to the presence of shot noise and

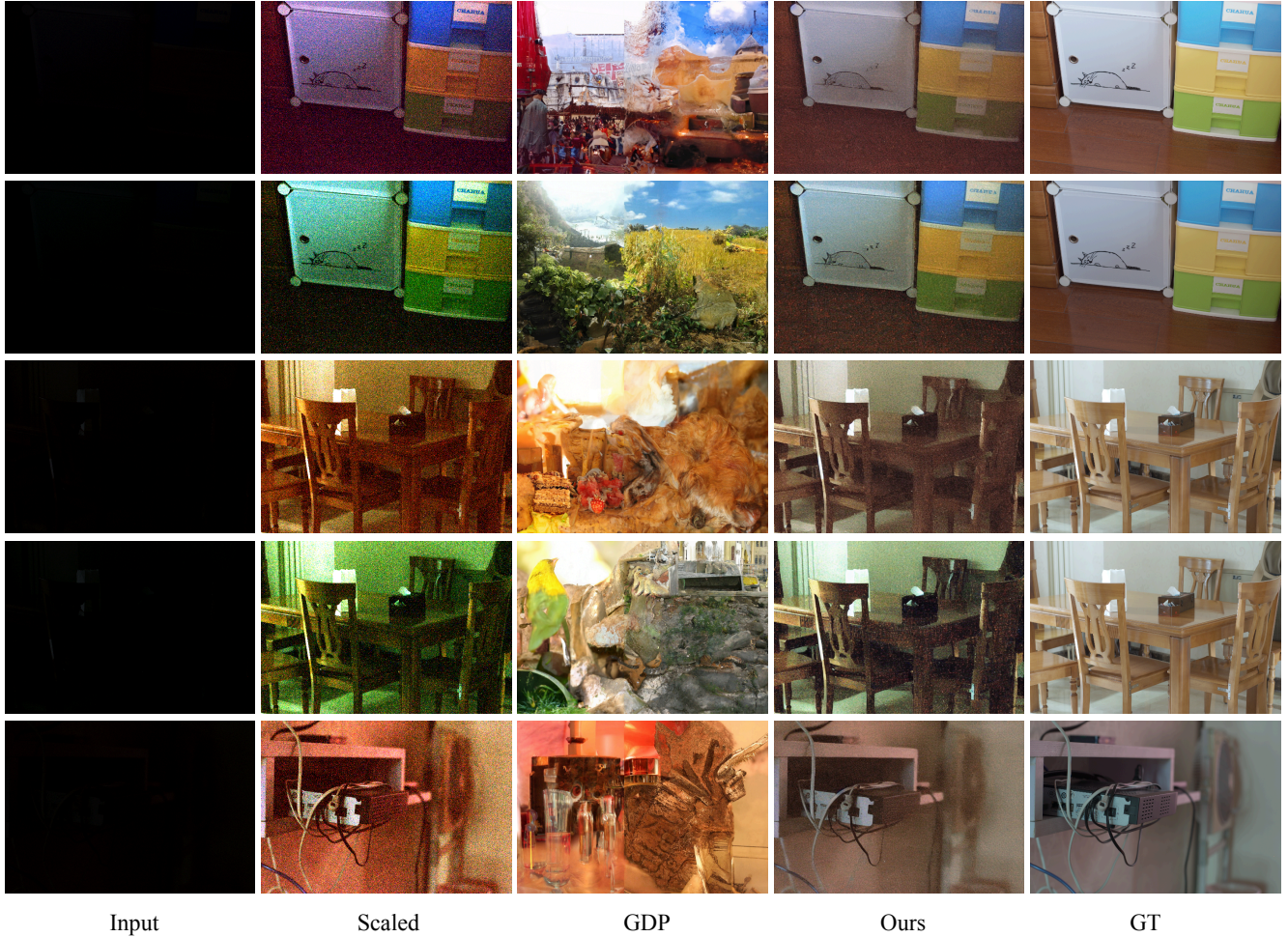


Figure 2. **Hallucination.** In the presence of substantial noise and darkness in input images, GDP often hallucinates by introducing non-existent objects or reconstructing completely different scenes. For example, a blue-colored cabinet is inaccurately reconstructed as a sky, a pink cabinet as a building, and the entire scene resembling a battle (row 1). It is clearly observable that GDP often hallucinates whereas our method exhibits consistency both with the ground truth and across different images of the same scene, underscoring the reliability and robustness of our approach. Moreover, our method produces clean and sharp outputs for less noisy inputs and effectively attenuates noise even in challenging cases involving severe darkness and pronounced noise levels. For additional examples, please refer to our supplemental.

color quantization effects, which undermine the applicability of elementary solutions such as uniform intensity scaling as evidenced in Figure 1 (first row, Scaled column).

Supervised learning methods have shown promising results in low-light image enhancement. However, current state-of-the-art methods often perform optimally only on the datasets they were trained on, thereby constraining their generalizability. This constraint arises primarily due to the scarce paired low and normal light images and limited diversity present in the training datasets. As shown in Figure 1, Retinexformer, a leading supervised method trained on the LOL dataset [51], exhibits inconsistent reconstructions of the same candle scene (row 1 and row 2) from the MEF dataset [33] as well as pronounced warm orange color shifts in the bridge scene (row 3) from the NPE dataset [49].

Unsupervised learning methods [28, 42] have emerged as a promising direction for low-light and backlit image enhancement, as they do not rely on paired datasets. These approaches leverage statistical properties such as intensity distributions, color balance, and textural patterns to transform images into normal lighting conditions. However, their performance is fundamentally tied to the diversity of the training data. Limited variability in lighting scenarios and scene compositions can hinder the models’ ability to generalize, resulting in suboptimal adjustments for images outside their learned domain.

Recent effort [9] has applied diffusion models, which draw on priors formed from extensive collections of well-lit images to define how a properly illuminated image should appear, to low light enhancement tasks in a zero-

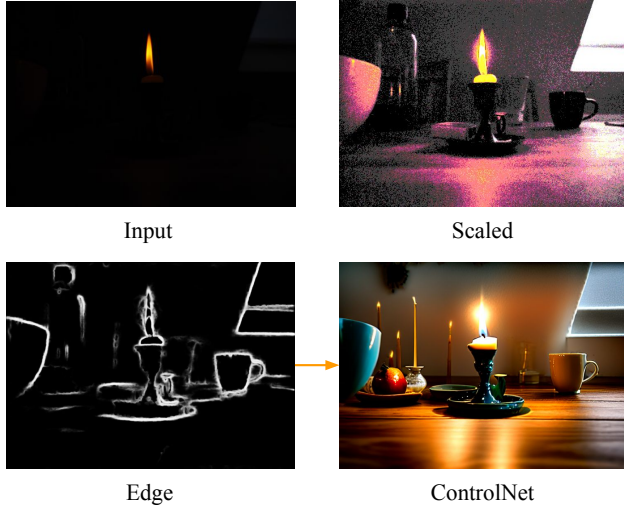


Figure 3. Applying ControlNet [59], an edge-conditioned text-to-image diffusion model, in the domain of low light image enhancement. The ControlNet image is generated with the prompt “a tranquil indoor scene featuring a lit candle on a wooden dining table, surrounded by a white bowl, a black coffee mug, and a water bottle, with a window in the background casting a soft light, photorealistic, 8k”. For visualization, the scaled image corresponds to the input image uniformly scaled to an average intensity of 140.0. Given an edge map from HED [52] derived from the scaled image, ControlNet produces a noise-free, high-resolution normal-light image. While edge maps effectively capture global structures, they fall short in preserving fine-grained structural details and ensuring chromatic fidelity. Furthermore, accurate prompt engineering is often laborious, and ControlNet often does not consistently produce outputs that align with the described scenes. For example, ControlNet erroneously interprets the disjoint edges of the water bottle as multiple candles in the top left. Similarly, areas lacking edge detail result in the unintended generation of artifacts such as apples and plates. The bowl and coffee mug in the output also exhibit colors that diverge from the original description. In this work, we show that self-attention features of an input low-light image serve as a complementary modality to ControlNet, enriching the information that edge maps alone cannot fully encapsulate. Our method does not require a prompt, due to its negligible effect, and please refer to row 1 in Figure 1 to see our reconstruction result.

shot framework. While diffusion models are adept at generating visually realistic content, they are prone to “hallucination” under conditions of limited information, such as extremely dark images characterized by significant noise. This phenomenon is illustrated in Figure 1, where GDP [9], a diffusion-based method, exhibits severe hallucinations when processing extremely low-light inputs with noise.

In this paper, we demonstrate that effective enhancement hinges on capturing and preserving essential features of the input low-light image. By leveraging these features to adjust the self-attention in a pre-trained diffusion model, our

method achieves low-light image enhancement that: (a) requires no paired data; (b) achieves competitive performance with paired-data models on paired datasets; (c) outperforms existing diffusion-based method; and (d) avoids hallucination, even in cases of exceptionally dark images with noise.

Our approach is based on ControlNet [59] to produce a high-quality, well-exposed image, with the generation process conditioned on an edge map derived from the low-light input. This edge map, while capturing the global structural essence of the scene, fails to retain the nuanced color and fine-grained structural information of the input, thereby not fully preserving the structural integrity and color fidelity of the original scene in the resultant images. Therefore, guiding ControlNet to render a well-illuminated counterpart necessitates the integration of essential cues extracted from the low-light input image.

Plug-and-Play [48], a text-driven image-to-image translation framework, has demonstrated that leveraging residual features and self-attention maps enables the generation of a new image that adheres to the provided text while retaining the semantic structure of the input guidance image. Inspired by this approach, we guide the generation process of ControlNet which is conditioned on the edge map derived from its low-light input image with its self-attention features but without requiring text prompts. Through this approach, we show that self-attention features serve as a complementary modality to ControlNet, enriching the information that edge maps from low-light inputs cannot fully encapsulate.

We further demonstrate that fine-tuning ControlNet through Low-Rank Adaptation (LoRA) [19] with the input low-light image itself as the reconstruction target as well as noise initialization through AdaIN [20], is essential for retaining the spatial and color fidelity of the input image, as highlighted in Figure 5 and Figure 6.

#### Our key contributions are as follows:

1. We introduce an effective zero-shot method that requires only the input image itself, avoiding the dependency on paired low and normal light images, thereby ensuring independence from specific datasets.
2. We achieve consistency with the ground truth and across images of the same scene under varying illumination, highlighting the reliability and robustness of our method.
3. We integrate a series of control techniques, including Plug-and-Play [48], ControlNet [59], and noise initialization through AdaIN [20], to preserve the original image’s intrinsic color and spatial integrity, effectively reconstructing scenes without introducing artifacts and hallucinations.
4. Through extensive quantitative and qualitative evaluations, we demonstrate that our zero-shot approach attains superior performance in low-light image enhancement tasks.

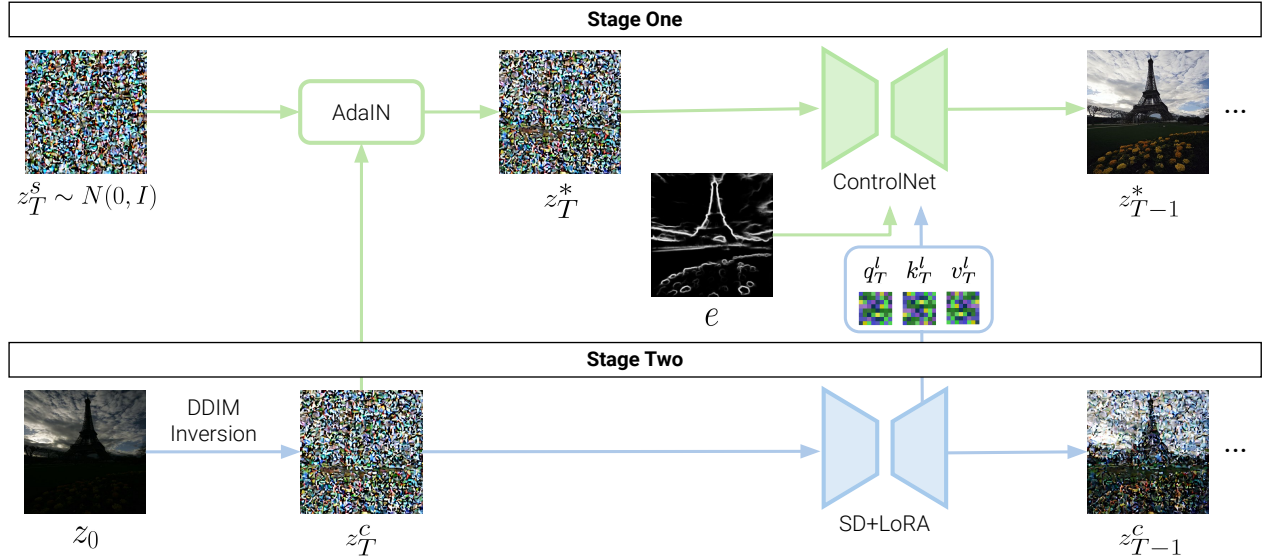


Figure 4. **Stage One:** We initiate the standard image generation process of the ControlNet, which synthesizes a noise-free and naturally illuminated image conditioned on an edge map  $e$  as shown in Figure 3. To impose enhanced spatial constraints derived from the input, while excluding noise and brightness attributes, we employ AdaIN on the DDIM-inverted latent representation of the input image,  $z_T^c$ , as content and a random noise,  $z_T^s$ , as style. This forms the initial latent input for the frozen ControlNet. While the diffusion prior aids in generating a normally-lit image, accurately uncovering inherent colors of the scene demands the integration of additional information. **Stage Two:** To derive this information, we fine-tune Stable Diffusion with LoRA on an input image, followed by a denoising process to extract self-attention features from the decoder layers at each timestep  $t \in \{1, \dots, T\}$ . These features serve to bias the ControlNet inference. Our method employs LoRA fine-tuning with the input image itself, given that the precision of our method hinges on self-attention features derived from the correct denoising process to achieve self-reconstruction, as depicted in Figure 5. The self-attention features are then injected into the corresponding ControlNet decoder layers at each timestep. We hypothesize, corroborated by experimental results, that self-attention features prove effective for low-light image enhancement because they provide long-scale spatial support and the chromatic features are largely unaffected by brightness and noise variations.

## 2. Related Work

Traditional image enhancement methods, including histogram equalization [13, 39] and gamma correction [41], rely on global adjustments to enhance image contrast. Despite their computational efficiency, these methods are inherently limited by their inability to account for varying scene-specific lighting conditions. Moreover, their global adjustment inadvertently amplifies dark noise in low-light areas, diminishing fine details and introducing artifacts.

Convolutional Neural Networks (CNNs) are adept at learning transformations from under-exposed to well-lit images, effectively capturing local textures and patterns [10, 31, 51, 56]. However, CNNs often fall short of capturing long-range dependencies. To address this limitation, an ensemble method [2] uses large-scale estimates for noise removal in dark regions and small-scale estimates to restore details in bright areas. Likewise, Retinexformer [3] introduces illumination-guided attention to capture long-range dependencies to overcome the limitations of CNNs. Despite these advances, reliance on scarce paired datasets for supervised training constrains their ability to generalize ef-

fectively.

To address the limited availability of paired low-light and normal-light image datasets, approaches such as [1] and [37] generate synthetic low-light images derived from well-lit images. While synthetic data is more abundant than real paired datasets, its use in supervised training constrains model generalization to unseen, real-world dark images.

Recently, generative methods have exhibited promising results in low-light image enhancement, with diffusion models [6, 16, 43, 44, 46, 47] demonstrating particular efficacy due to their strong generative ability, being free from the instability and mode-collapse problems that are prevalent in previous generative models such as generative adversarial networks (GANs) and variational autoencoders (VAEs). However, standard Gaussian noise assumptions of diffusion models do not model the complex noise of low-light images. In response, new training strategies have been proposed for LLIE [18, 21, 22, 30, 38, 50, 57]. However, these methods remain dependent on supervised learning, without leveraging the generative priors of the pre-trained diffusion models. GDP [9], a recent zero-shot diffusion-based approach, provides a pioneering solution to the afore-

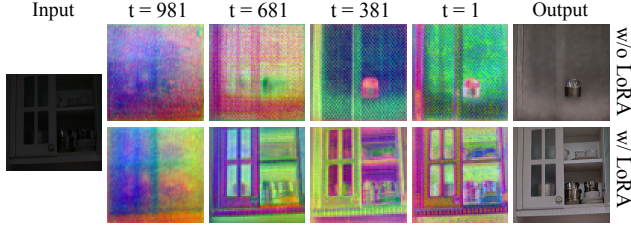


Figure 5. Self-attention visualization of the input image through PCA during the diffusion sampling sequence. It highlights the centrality of LoRA-finetuning as it enables the self-attention maps to capture structural and inherent chromatic subtleties of the scene, facilitating a more accurate final restoration. From the same input image, the top row visualizes the self-attention maps extracted from the diffusion model without LoRA, whereas the bottom row corresponds to the maps derived from the model fine-tuned with LoRA.

mentioned challenges by utilizing classifier guidance with a learnable degradation model. Nevertheless, its reliance on an assumed, predefined degradation process constrains its adaptability to unknown or complex degradations [55], and it is liable to hallucinate due to inadequate constraints on the diffusion model as shown in Figure 2. Concurrent with our work, FourierDiff [32] introduces a zero-shot diffusion-based approach by decomposing images into amplitude and phase components during the reverse diffusion process. This method leverages amplitude for brightness alignment and phase for content preservation, specifically addressing low-light blurry images. The reader is encouraged to review their work.

Several approaches have drawn upon the internal components of pre-trained diffusion models to achieve fine-grained control over outputs [4, 8, 14, 24, 48, 59]. For example, Prompt-to-Prompt [14] aligns the generated composition with the source prompt by leveraging its cross-attention maps from a pre-trained diffusion model during denoising with the target prompt. Similarly, Plug-and-Play [48] guides the generation process by using residual and self-attention features from an input image to facilitate text-driven image-to-image translation in pre-trained diffusion models. Furthermore, previous studies [35, 58] demonstrate that structured noise initialization, as opposed to pure Gaussian noise with zero signal-to-noise ratio (SNR), improves the fidelity of diffusion model outputs in guided image editing and synthesis tasks. For example, PCA-K Offset Training [58] introduces a PCA-derived component to the initial noise, while SDEdit [35] derives its initial noise from the input image, thereby preserving compositional coherence.

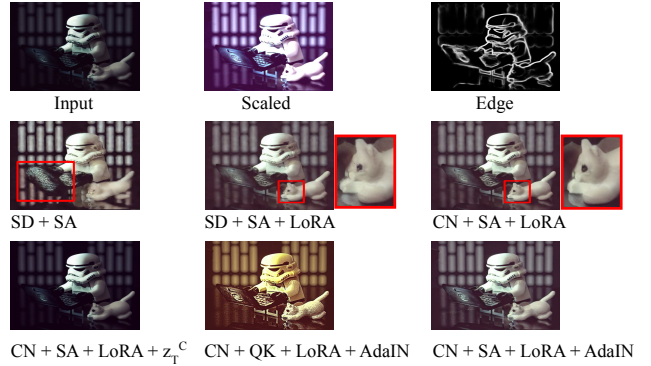


Figure 6. Qualitative ablation study to assess the individual and combined contributions of components. **SD**: Stable Diffusion, **CN**: ControlNet, **LoRA**: LoRA fine-tuning with an input low-light image, **SA**: Self-Attention injection from an input image to ControlNet decoder layers across all denoising timesteps, **QK**: Query and Key injection from an input image to ControlNet decoder layers across all denoising timesteps,  $z_T^C$ : noise initialization with a noised latent representation of the input image, **AdaIN**: noise initialization with AdaIN between  $z_T^C$  and a sampled  $z_T^S \sim \mathcal{N}(0, I)$ . The first four methods are initialized with a randomly sampled noise from  $\mathcal{N}(0, I)$ . For quantitative comparison, please refer to our Supplemental.

## 3. Method

### 3.1. Stage One: ControlNet-driven image synthesis with initialized noise

Our framework comprises two stages. In Stage One, we initiate the image generation process with ControlNet, to produce a noise-free, normally illuminated image that conforms to the global structural condition outlined by the edge map  $e$  as shown in Figure 3. This approach stands apart from conventional methods that focus on learning the mapping of the dark inputs directly into their lit equivalents. To derive the edge map  $e$ , we employ HED [52] due to its robustness in extracting edges from low-light images in the presence of noise. By comparison, Canny and Sobel edge detectors are susceptible to noise and demand precise threshold tuning to be effective.

Previous studies [35, 58] suggest that initializing the noise at inference with structured data, rather than purely white noise from  $\mathcal{N}(0, I)$ , helps retain the structure of the input image. However, as presented in Figure 6, initializing with  $z_T^C$ , a noised latent representation of the input  $x^c$  through DDIM inversion [45], generates an output that exhibits minimal distinction from the input image. This is because both the initial noise and self-attention features are derived from the same low-light image. Conversely, initializing with randomly sampled noise yields an output that more closely resembles the ground truth, because ControlNet has been trained on a vast set of well-exposed im-

---

**Algorithm 1**

---

```
1: Input:  $x^c$ : Low-light input image.
2: if  $\bar{x}^c < \tau_{\text{avg}}$  then  $x^c \leftarrow x^c \times \left(\frac{\tau_{\text{avg}}}{\bar{x}^c}\right)$ 
3:  $e \leftarrow \text{HED}(x^c)$  ▷ Edge condition
4:  $z_T^c \leftarrow \text{DDIM-inv}(x^c)$ 
5:  $z_T^s \leftarrow \epsilon \sim \mathcal{N}(0, I)$ 
6:  $z_T^* \leftarrow \sigma(z_T^s) \left(\frac{z_T^c - \mu(z_T^c)}{\sigma(z_T^c)}\right) + \mu(z_T^s)$  ▷ AdaIN
7:
8:  $\epsilon_{\theta+\Delta\theta} \leftarrow \text{LoRA}(z^c, \epsilon_\theta)$  ▷ LoRA fine-tuning
9:
10: for  $t = T \dots 1$  do
11:    $\epsilon_{t-1}^c, A_t^l \leftarrow \epsilon_{\theta+\Delta\theta}(z_t^c, t)$ 
12:    $A_t^{*l} \leftarrow A_t^l$  ▷ Self-attention injection
13:    $\epsilon_{t-1}^* \leftarrow \epsilon_{\theta_{\text{cn}}}(z_t^*, t; e, A_t^{*l})$ 
14:    $z_{t-1}^* \leftarrow \text{DDIM-samp}(z_t^*, \epsilon_{t-1}^*)$ 
15: end for
16: Output:  $I^* \leftarrow z_0^*$ 
```

---

ages with random initial noise. However, in diffusion models, the initial noise largely dictates what is generated, and any discordance between the injected self-attention features and the evolving latent representation may result in loss of detail, as depicted in Figure 6. In response, we perform AdaIN [20] style transfer on  $z_T^c$  using a style reference from a randomly initialized noise  $z_T^s \sim \mathcal{N}(0, I)$  to impose enhanced spatial constraints derived from the input while excluding noise and brightness attributes:

$$z_T^* = \sigma(z_T^s) \left(\frac{z_T^c - \mu(z_T^c)}{\sigma(z_T^c)}\right) + \mu(z_T^s)$$

This approach effectively retains the original image’s salient characteristics while initializing the generation with a clean, well-lit latent.

To evaluate the effect of the AdaIN operation, we inject only the query and key (QK). The resulting attention map from this query-key combination preserves the structure of the input low-light image while maintaining chromatic attributes from AdaIN. While the output image reflects partial color fidelity from the input and resembles the brightness of well-exposed images, it suffers from a noticeable color shift, evident from the warm, orange tint seen in the generated image (CN + QK + LoRA + AdaIN in Figure 6). This reflects the necessity of retrieving the intrinsic color characteristics of the scene from the input image and effectively incorporating them to guide ControlNet’s generation process.

### 3.2. Stage Two: Self-Attention Features as Guidance for ControlNet

To capture essential features of the input low-light image to guide the generation process of ControlNet, we draw upon

the internal components of pre-trained diffusion models that are available during the DDIM sampling phase to achieve fine-grained control over ControlNet.

While the denoising process yields a comprehensive array of features, only a critical subset demonstrates genuine pertinence to our objective. As the self-attention computation quantifies the affinity between queries and keys and captures the spatial relationships within the input, several works [24, 48] have leveraged the self-attention features within pre-trained diffusion model for spatial control over the generated image. Additionally, it has been empirically shown that self-attention not only captures spatial attributes but also retains rich color information, thereby facilitating style transfer applications [5, 15]. In our task, we hypothesize, corroborated by experimental results, that self-attention features prove effective for low-light image enhancement because they provide long-scale spatial support and the chromatic features are largely unaffected by brightness and noise variations. Therefore, we leverage the self-attention features as a complementary modality to ControlNet, enriching the information that edge maps from low-light inputs cannot fully encapsulate. Specifically, we extract the self-attention features from each layer  $l$  of the decoder across all timesteps  $t \in \{1, \dots, T\}$ , with  $T = 50$ :

$$A_t = \text{Softmax} \left(\frac{q_t(k_t)^\top}{\sqrt{d}}\right) v_t$$

, where  $q_t^l$ ,  $k_t^l$ , and  $v_t^l$  are the query, key, and value embeddings respectively, and  $d$  represents the dimensionality of the key and query embeddings.

The encoder in the frozen ControlNet remains intact while we modify only the decoder by injecting the extracted self-attention features into ControlNet  $\epsilon_{\theta_{\text{cn}}}$  as follows:

$$\epsilon_{t-1}^* \leftarrow \epsilon_{\theta_{\text{cn}}}(z_t^*, t; e, A_t^{*l})$$

Here,  $e$  represents the edge map conditioning input (depicted in Figure 6),  $\epsilon_{t-1}^*$  is the predicted noise to estimate the latent at timestep  $t - 1$ , and  $A_t^{*l}$  is the injected self-attention features extracted from the input image at timestep  $t$ . Therefore, our method guides the generation process of ControlNet with the self-attention features derived from the low-light input image as a complementary modality to ControlNet, enriching the information that edge maps alone cannot fully encapsulate.

However, we empirically observe that extracting self-attention features of the input during naive DDIM sampling performs suboptimally on low-light images, as illustrated by the kitchen cabinet example in Figure 5. To mitigate this, we fine-tune the pre-trained diffusion model using a parameter-efficient approach, LoRA [19], aiming to accurately self-reconstruct the low-light image  $x^c$  through fine-tuning. This adjustment facilitates the stability of our

Methods	LOL							LOLv2							
	PSNR $\uparrow$	SSIM $\uparrow$	LPIPS $\downarrow$	MS-SSIM $\uparrow$	VIF $\uparrow$	FSIM $\uparrow$	DISTS $\downarrow$	PSNR $\uparrow$	SSIM $\uparrow$	LPIPS $\downarrow$	MS-SSIM $\uparrow$	VIF $\uparrow$	FSIM $\uparrow$	DISTS $\downarrow$	
S	KinD [61]	17.648	0.775	0.175	0.924	0.498	0.920	0.128	20.588	0.820	0.143	0.932	0.508	0.928	0.129
	KinD++ [62]	17.752	0.766	0.198	0.859	0.366	0.866	0.150	17.660	0.770	0.216	0.839	0.371	0.847	0.182
	SNR [53]	24.609	0.842	0.151	0.965	0.565	0.958	0.140	21.479	<b>0.849</b>	0.157	0.951	<b>0.528</b>	0.953	0.136
	GSAD [17]	22.690	<b>0.851</b>	<b>0.103</b>	0.964	<b>0.592</b>	<b>0.961</b>	<b>0.092</b>	20.292	0.846	<b>0.113</b>	<b>0.954</b>	<b>0.528</b>	<b>0.955</b>	<b>0.104</b>
	Retinexformer [3]	<b>25.153</b>	0.845	0.131	<b>0.970</b>	0.517	<b>0.961</b>	0.138	<b>22.794</b>	0.840	0.171	<b>0.954</b>	0.489	0.954	0.159
U	RUAS [42]	16.405	0.500	0.270	0.872	0.401	0.884	0.189	13.975	0.466	0.340	0.837	0.594	0.898	0.232
Z	SCI [34]	14.784	0.522	0.339	0.890	<b>0.436</b>	0.911	0.211	17.304	0.534	0.308	0.901	<b>0.445</b>	0.923	0.202
	Zero-DCE [11]	14.861	0.559	0.335	0.895	0.420	<b>0.918</b>	0.216	18.059	0.574	0.313	<b>0.909</b>	0.425	<b>0.926</b>	0.204
	GDP [9]	15.793	0.540	0.343	0.829	0.279	0.854	0.190	14.494	0.498	0.358	0.794	0.284	0.832	0.217
	Ours	<b>17.278</b>	<b>0.680</b>	<b>0.232</b>	<b>0.902</b>	0.250	0.896	<b>0.162</b>	<b>20.093</b>	<b>0.660</b>	<b>0.244</b>	0.865	0.209	0.879	<b>0.174</b>

Table 1. Quantitative comparison on the LOL [51] and LOLv2 Real [56] dataset. The best results are highlighted in red. Our model produces outputs at a resolution of  $512 \times 512$ , which are resized to the original resolution ( $400 \times 600$ ) for a fair comparison against the ground truth. The notation (S) indicates supervised methods trained on LOL, (U) denotes unsupervised methods, and (Z) represents Zero-Shot approaches, including ours.

Methods	DICM			MEF			LIME			NPE			VV			
	NIQE $\downarrow$	PIQE $\downarrow$	ILNIQE $\downarrow$	NIQE $\downarrow$	PIQE $\downarrow$	ILNIQE $\downarrow$	NIQE $\downarrow$	PIQE $\downarrow$	ILNIQE $\downarrow$	NIQE $\downarrow$	PIQE $\downarrow$	ILNIQE $\downarrow$	NIQE $\downarrow$	PIQE $\downarrow$	ILNIQE $\downarrow$	
S	KinD [61]	3.298	48.862	25.698	3.623	56.091	32.417	<b>3.581</b>	49.137	<b>26.821</b>	<b>3.345</b>	41.726	<b>24.034</b>	<b>2.887</b>	49.484	22.764
	KinD++ [62]	3.242	44.425	<b>23.15</b>	3.57	55.305	27.797	3.984	45.561	27.015	3.57	42.149	24.637	2.992	48.747	<b>21.23</b>
	SNR [53]	3.824	48.095	26.567	3.956	52.577	31.457	4.578	45.544	30.778	4.099	42.825	27.855	3.706	42.474	24.44
	GSAD [17]	3.94	44.056	24.365	3.804	48.259	28.946	4.577	39.194	28.342	4.196	40.333	24.843	4.868	36.223	24.148
	Retinexformer [3]	<b>3.235</b>	<b>29.658</b>	23.556	<b>3.474</b>	<b>35.065</b>	<b>27.327</b>	4.062	<b>31.609</b>	27.572	3.727	<b>31.562</b>	25.556	3.178	<b>26.726</b>	21.822
U	RUAS [42]	4.514	39.097	39.423	5.062	42.68	41.777	4.29	40.776	33.92	5.84	51.272	42.001	3.817	36.784	35.319
Z	SCI [34]	3.685	36.424	29.9	4.005	36.504	29.98	4.114	36.729	28.87	3.848	38.484	27.659	2.313	25.81	25.928
	Zero-DCE [11]	<b>3.325</b>	34.834	27.601	4.030	35.888	29.253	3.792	34.093	28.527	3.424	33.069	<b>24.637</b>	<b>2.165</b>	<b>19.428</b>	23.621
	GDP [9]	3.354	28.17	26.69	<b>3.495</b>	36.508	31.728	3.784	33.375	28.901	<b>3.299</b>	32.153	25.44	2.959	33.832	25.462
	Ours	3.632	<b>24.743</b>	<b>24.946</b>	3.897	<b>26.337</b>	<b>25.663</b>	<b>3.718</b>	<b>26.515</b>	<b>23.068</b>	3.761	<b>24.898</b>	24.877	3.426	26.949	<b>23.383</b>

Table 2. A quantitative comparison on unpaired datasets. The best results are highlighted in red. Metrics are computed directly from the original model outputs for each method without resizing due to the high occurrence of high-resolution images (e.g.,  $2304 \times 1728$ ) in the NPE and VV datasets. For results using resized outputs matched to the ground-truth resolution, please refer to the Supplemental. (S) refers to supervised methods trained on LOL, (U) indicates unsupervised methods, and (Z) represents Zero-Shot approaches, including ours.

method by enabling precise reconstruction of the low-light input  $x^c$  and accurate extraction of self-attention features  $A_t^l$  during denoising, as presented in Figure 5. Therefore, in contrast to prior works [5, 15, 24, 48] that rely on the raw self-attention features directly derived from the input image, our approach leverages LoRA-adjusted self-attention features. This refinement enhances the self-attention features, improving their precision in portraying subtle structural and chromatic details, as depicted in Figure 5. For preprocessing, we upscale the average intensity of the low-light image  $x^c$  to a threshold  $\tau_{\text{avg}} = 40$  if the original intensity is below this level. This adjustment improves visibility without inducing excessive noise amplification. However, we exclusively increase  $\tau_{\text{avg}}$  to 70.0 when extracting edges as  $z^c \leftarrow \text{HED}(x^c)$ , to improve image visibility, leveraging HED’s robustness to noise and its ability to accurately detect global edges.

## 4. Experiments

**Datasets.** We evaluate the performance of our method on widely used low-light datasets. Our experiments are con-

ducted on the LOL [51] test set and LOLv2 [56] test set to facilitate comprehensive quantitative and qualitative comparisons with representative state-of-the-art methods. The LOL dataset comprises 500 images, with 15 reserved for testing. LOLv2 consists of Real and Synthetic subsets, with training and testing splits of 689:100 for the Real subset and 900:100 for the Synthetic subset. The Synthetic subset was synthesized by adjusting the Y channel in the YCbCr color space to replicate low-light histogram characteristics. As our primary focus lies on the Real subset, which contains intrinsic noise, we report metrics on the Real test set to provide a robust evaluation of low-light performance. We also compare on five standard unpaired benchmarks: DICM [25] (44 test images), LIME [12] (10 test images), NPE [49] (75 test images), MEF [33] (79 test images), and VV<sup>1</sup> (24 test images).

**Metrics.** For the paired LOL dataset, which includes a reference ground truth image, we employ seven reference-based image quality assessment metrics: Peak Signal-to-

<sup>1</sup><https://sites.google.com/site/vonikakis/datasets>



Figure 7. Qualitative evaluation of our method against existing unsupervised and zero-shot approaches on the paired LOL [51] dataset. While these methods perform adequately in cases requiring minimal scaling adjustments (row 4 and Figure 9), they fail to address complex inputs with significant darkness and noise (motorcycle scene in row 2). For example, GDP introduces hallucinated artifacts under high levels of darkness and noise (row 1), and as evidenced across all rows, the outputs from each method resemble uniform global intensity adjustments. Please zoom in for a detailed comparison.

Noise Ratio (PSNR) to quantify signal strength relative to noise, Structural Similarity (SSIM) and Multi-Scale SSIM (MS-SSIM) to assess coarse and fine structural details, Feature Similarity (FSIM) to evaluate the key image features such as edges and textures, and Visual Information Fidelity (VIF) to measure the visual information retained in the image. Higher values indicate greater similarity between model prediction and the ground truth. Additionally, we use deep learning-based metrics - Learned Perceptual Image Patch Similarity (LPIPS) [60] and Deep Image Structure and Texture Similarity (DISTS) [7] - which assess perceptual similarity. For these metrics, lower values correspond to higher perceptual quality.

In the context of unpaired datasets, which do not include reference ground truth images, we evaluate image quality using three no-reference metrics: NIQE [36], PIQE, and ILNIQE. Lower scores across these metrics denote superior image quality.

**Baseline methods.** We benchmark our proposed method with three categories of existing methods: (1) *supervised* methods trained on paired datasets, including KinD [61], KinD++ [62], GSAD [17], RetinexFormer [3], and

SNR [53]; and (2) *unsupervised* and (3) *zero-shot* methods, including RUAS [42], GDP [9], SCI [23], and Zero-DCE [11]. To facilitate a fair evaluation, we rely on the official code and pre-trained weights released by the respective authors. Supervised methods are trained on the LOL train set for evaluation on the LOL test set. For the LOLv2 Real test set, pre-trained weights on LOLv2 Real are used, with the exception of KinD [61] and KinD++ [62], which are trained on LOL. While the LOL and LOLv2 datasets differ, a notable overlap of images between them accounts for the high-performance metrics observed for KinD and KinD++. For unpaired dataset evaluation, model checkpoints trained on the LOL train set are used to assess the generalizability of the supervised approaches.

#### 4.1. Experimental Results

**Quantitative Results on Paired Data.** We begin by evaluating our method in comparison to all other methods on the LOL [51] and LOLv2 [56] test sets. As highlighted in Table 1, our approach consistently outperforms existing unsupervised and zero-shot methods in most quantitative metrics and achieves results comparable to supervised methods. Notably, our method improves upon the second-best zero-



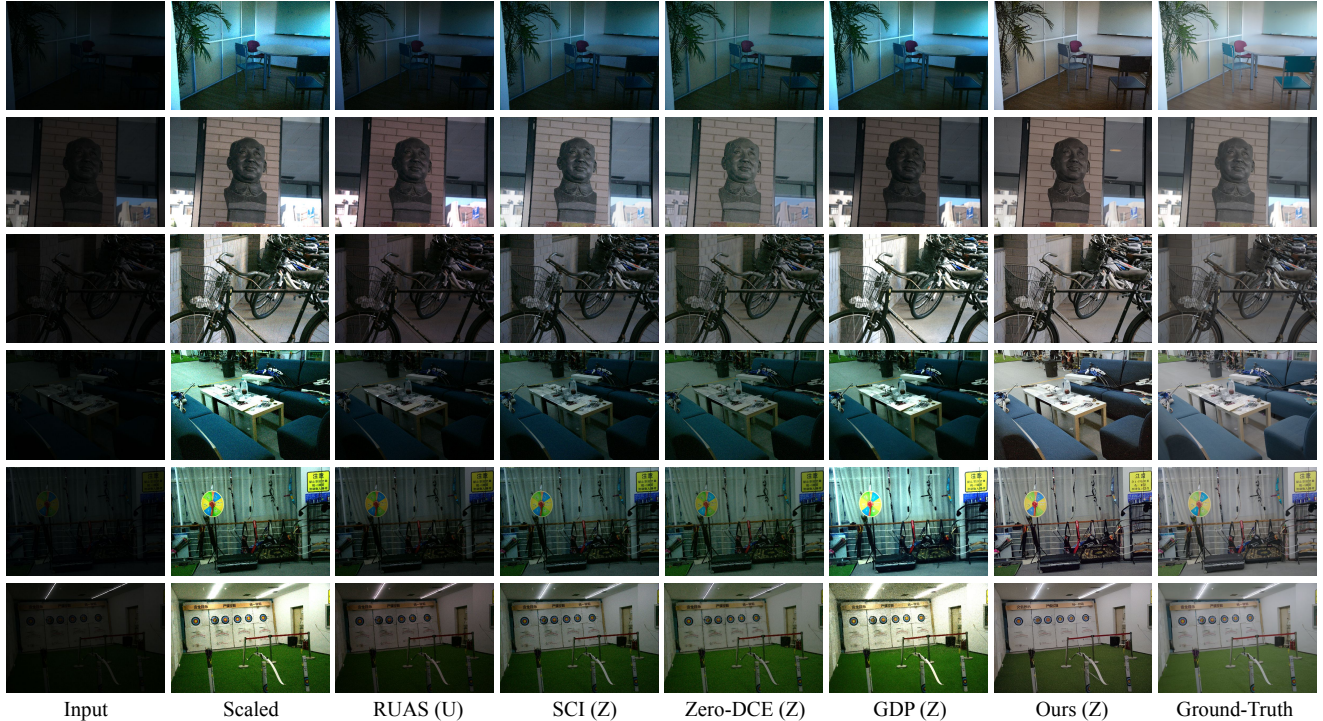


Figure 8. Qualitative evaluation of our method against existing unsupervised and zero-shot approaches on the paired LOLv2 Real [56] dataset. Existing methods predominantly exhibit behavior akin to uniform brightness scaling as shown in each row. For example, rows 1, 4, and 5 illustrate how these methods fail to capture the intrinsic scene colors, instead producing outputs that resemble uniform global intensity adjustments, resulting in pervasive blue (rows 1, 4, 5) across the scene. Please zoom in to observe amplified residual noise and details.

shot and unsupervised approaches by a margin of 1.485 dB in PSNR and 0.121 in SSIM on the LOL dataset, surpassing GDP and Zero-DCE, respectively. On the LOLv2 dataset, it achieves gains of 2.032 dB in PSNR and 0.086 in SSIM compared to the second-best zero-shot and unsupervised approach. For perceptual evaluation based on the LPIPS metric, our method delivers the lowest perceptual distance across both datasets among zero-shot and unsupervised methods, affirming its effectiveness in restoring images with high visual quality.

**Qualitative Results on Paired Data.** While supervised methods trained on the LOL and LOLv2 training sets predictably demonstrate superior performance compared to unsupervised and zero-shot methods, it is noteworthy that our approach can accurately discern the intrinsic colors of a scene. For example, as depicted in Figure 7, Figure 8, and Figure 10, naive intensity amplification in the presence of noise frequently results in undesirable color shifts, such as the unintended blue tint observed on the motorcycle (row 2 in Figure 7) and indoor archery range (row 5 in Figure 8). In contrast, our method, dependent solely on the model’s output without post-processing, scaling, or any additional adjustments, accurately identifies the intrinsic colors of the

scene, suggesting strong generalization even without direct training on the target data distribution.

**Quantitative Results on Unpaired Data.** For a comprehensive performance assessment, we extend our analysis to unpaired datasets. The results presented in Table 2 demonstrate that our method consistently outperforms supervised, unsupervised, and zero-shot approaches across most metrics. These findings, combined with its proven effectiveness on the LOL and LOLv2 datasets, emphasize the robustness and generalizability of our approach across diverse data distributions.

**Qualitative Results on Unpaired Data.** The unpaired datasets present images that are inherently brighter and exhibit significantly reduced noise levels compared to the LOL and LOLv2 datasets. These attributes simplify the enhancement task, requiring only minor scaling adjustments to achieve perceptually convincing results. However, this apparent success of unsupervised and zero-shot methods on unpaired datasets fails to translate to the LOL and LOLv2 datasets, where the intricate interplay of brightness, noise, and detail demands more sophisticated approaches. Conversely, the LOL and LOLv2 datasets, with their darker and noisier images, cause supervised methods such as Retinex-

former and GSAD to over-brighten and lead to color distortions. This is because these unpaired datasets exhibit luminance and noise characteristics absent in the training data. In contrast, our method demonstrates robust performance across varying lighting and noise conditions, achieving optimal brightness through region-specific adjustments while preserving the scene’s intrinsic color fidelity.

**Hallucinations in GDP reconstructions.** As evidenced by Table 1 and Table 2, GDP exhibits limited effectiveness in enhancing low-light images, particularly for the LOL and LOLv2 datasets, which are more demanding due to higher levels of noise and darkness. However, we wish to underscore that GDP, as our zero-shot diffusion-based baseline, remains a robust and versatile image restoration approach, applicable across a range of tasks beyond low-light enhancement. Figure 7, Figure 8, Figure 10 further demonstrate GDP’s effectiveness in brightening images where other unsupervised and zero-shot methods fall short, delivering solid performance, albeit with less precision compared to ours. The comparisons presented in Figures 2, 7, 8, and 10 are intended to highlight the limitation of leveraging diffusion models for LLIE tasks on particularly challenging inputs characterized by significant noise, where most existing methods, including GDP, are prone to failure. The instances of hallucinated outputs serve to illustrate the inherent challenges of leveraging diffusion models to enhance low-light images and our work aims to address these limitations and improve robustness under such adverse conditions.

## 5. Discussion and Conclusion

We introduced a novel zero-shot framework for enhancing low-light images that overcomes the limitations inherent in existing zero-shot, supervised, and unsupervised methods. Current methods exhibit limitations when addressing input images characterized by pronounced noise and limited intensity. In such challenging conditions, GDP often exhibits hallucinations. Meanwhile, supervised and unsupervised methods are often constrained by their dependence on limited, curated training datasets, which reduces their adaptability to diverse real-world scenarios. In contrast, our approach harnesses the diffusion prior to recover intrinsic scene colors and apply localized region-specific brightening, maintaining color fidelity and avoiding overexposure in well-lit areas without hallucinations.

Our framework outperforms existing methods in its current form but is restricted to processing images at a resolution of  $512 \times 512$  pixels. Extending the framework to handle higher resolutions effectively remains an open challenge and a promising direction for improving its practicality and generalizability.

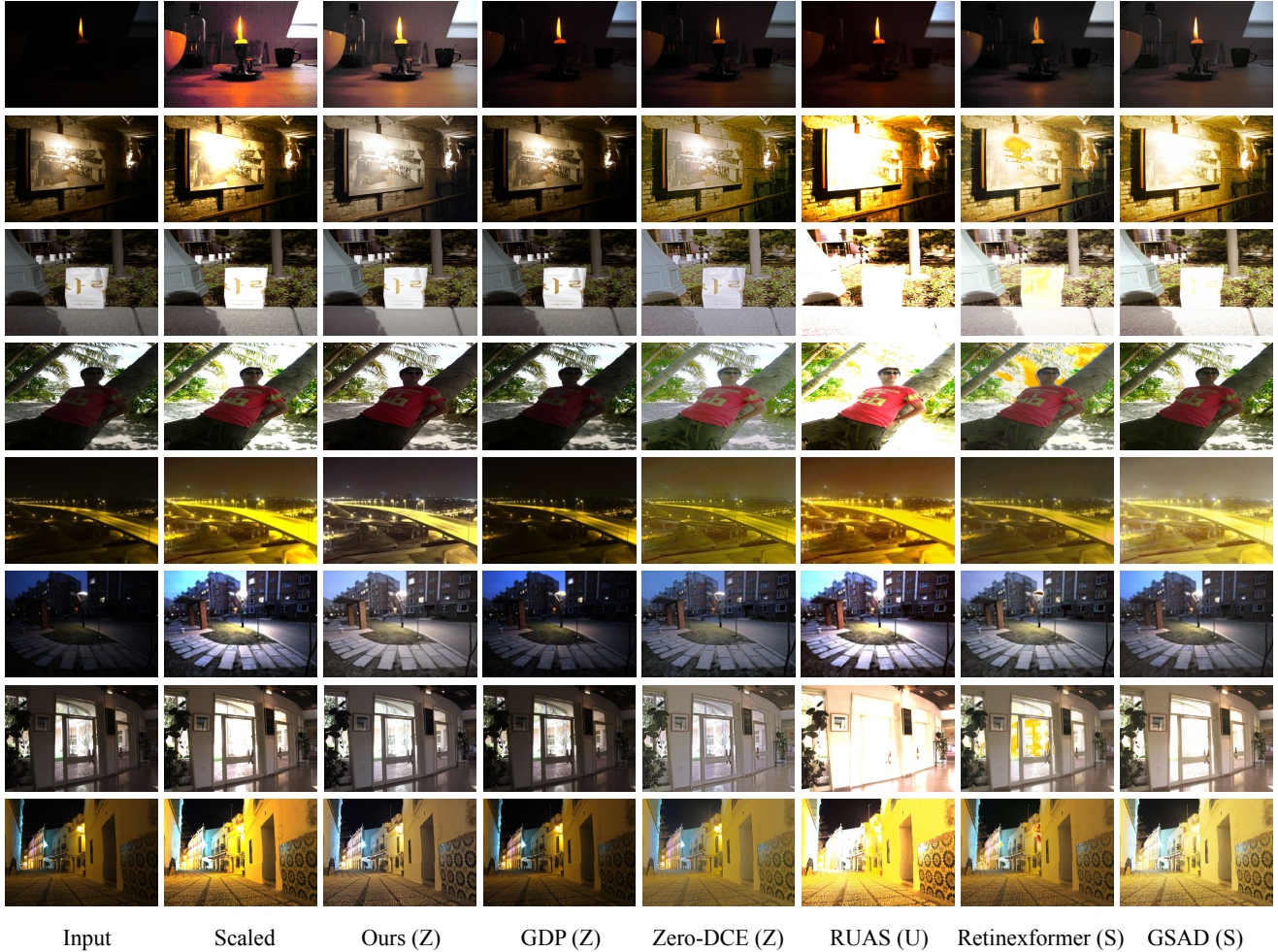


Figure 9. Qualitative results from the state-of-the-art methods on the unpaired datasets. Our diffusion-prior-based method adeptly balances illumination to a neutral level, in contrast to the baseline GDP, which fails to enhance dark regions adequately and resembles a uniform global scaling adjustment. For example, row 2 illustrates how our approach differs from uniform global scaling (Scaled), achieving *region-specific* brightening without overexposing already well-lit regions. Compared to the LOL and LOLv2 datasets, images in the unpaired datasets are notably brighter and exhibit negligible noise, where small scaling adjustments are often sufficient for optimal results. Consequently, supervised methods trained on LOL, such as Retinexformer and GSAD, demonstrate limited generalization capabilities. Their reconstructions frequently exhibit over-exposure (rows 2, 3, and 7) and pronounced color shifts (row 5) while failing to achieve region-specific brightening. Instead, they produce results resembling global uniform scaling. Furthermore, reported high metric scores for both Retinexformer and GSAD imply similar reconstruction quality, yet the outputs reveal notable discrepancies, as observed in each row. This implies that at least one, if not both, are overfitted to incorrect or irrelevant features to make predictions. From top to bottom, the image is associated with the following datasets: MEF, DICM, DICM, VV, NPE, LIME, MEF, LIME. Please zoom in for detailed comparison.

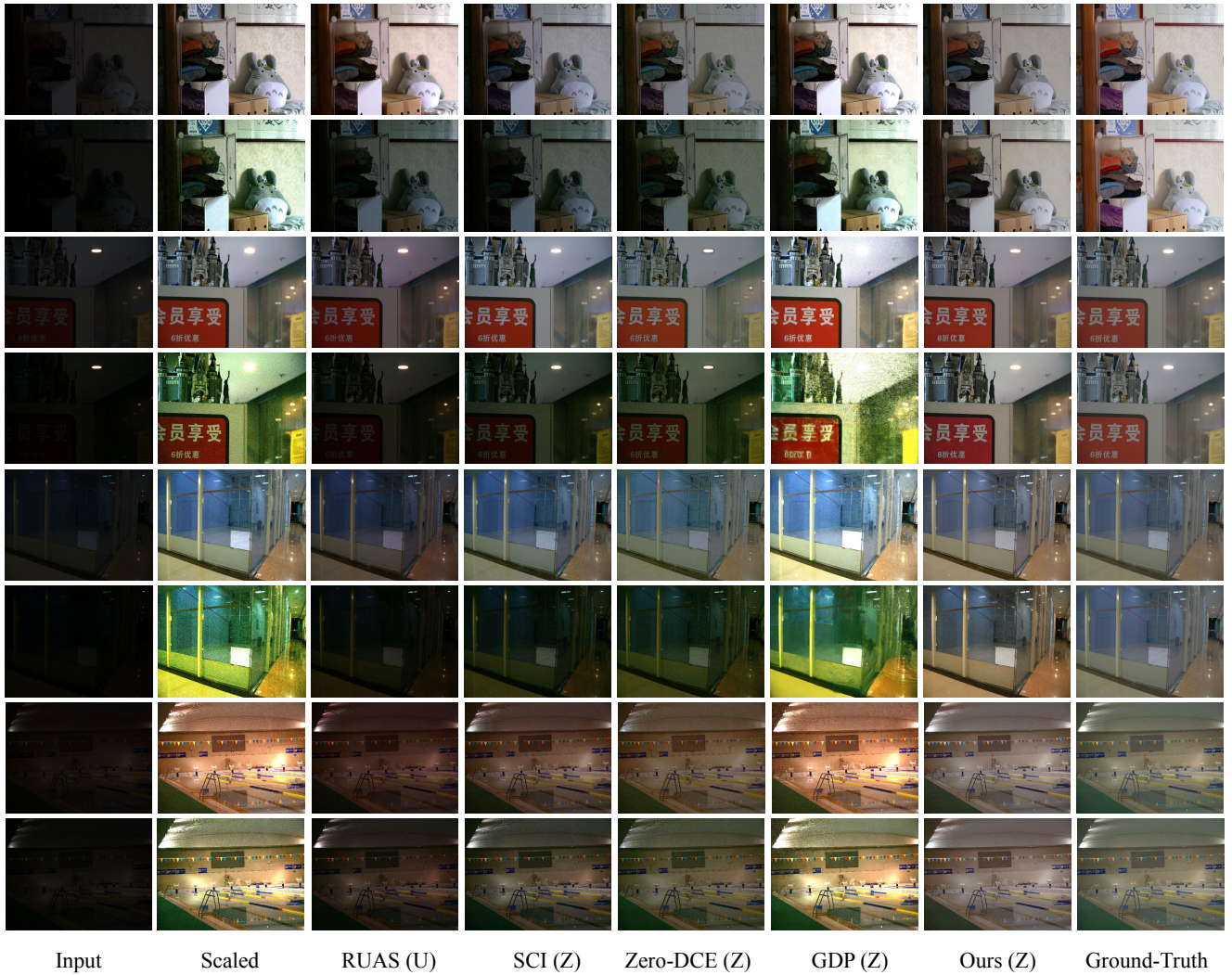


Figure 10. Qualitative evaluation of our method against existing unsupervised and zero-shot approaches on the paired LOL [51] and LOLv2 Real [56] dataset. Under varying noise and illumination levels, our method consistently reconstructs images of the same scene, whereas existing approaches suffer from pronounced variability. For example, competing methods often fail to adequately brighten the image or yield outputs with minor scaling adjustments, falling short of the expected consistency. In contrast, our method reliably delivers consistent results, effectively removes noise, and restores the intrinsic colors of the scene. Please zoom in to observe amplified residual noise and details.

## References

- [1] Sara Aghajanzadeh and David Forsyth. Towards robust low light image enhancement. *arXiv preprint arXiv:2205.08615*, 2022. 4
- [2] Sara Aghajanzadeh and David Forsyth. Long scale error control in low light image and video enhancement using equivariance. *arXiv preprint arXiv:2206.01334*, 2022. 4
- [3] Yuanhao Cai, Hao Bian, Jing Lin, Haoqian Wang, Radu Timofte, and Yulun Zhang. Retinexformer: One-stage retinex-based transformer for low-light image enhancement. In *ICCV*, pages 12470–12479. IEEE, 2023. 4, 7, 8
- [4] Mingdeng Cao, Xintao Wang, Zhongang Qi, Ying Shan, Xiaohu Qie, and Yinqiang Zheng. Masactrl: Tuning-free mutual self-attention control for consistent image synthesis and editing. In *ICCV*, 2023. 5
- [5] Jiwoo Chung, Sangeek Hyun, and Jae-Pil Heo. Style injection in diffusion: A training-free approach for adapting large-scale diffusion models for style transfer. In *Proceedings of the IEEE/CVF Conference on Computer Vision and Pattern Recognition (CVPR)*, pages 8795–8805, 2024. 6, 7
- [6] P. Dhariwal and A. Nichol. Diffusion models beat gans on image synthesis. In *Advances in Neural Information Processing Systems*, pages 8780–8794, 2021. 4
- [7] Keyan Ding, Kede Ma, Shiqi Wang, and Eero P. Simoncelli. Image quality assessment: Unifying structure and texture similarity. *IEEE Trans. Pattern Anal. Mach. Intell.*, 44(5): 2567–2581, 2022. 8
- [8] Dave Epstein, Allan Jabri, Ben Poole, Alexei A. Efros, and Aleksander Holynski. Diffusion self-guidance for controllable image generation. In *NeurIPS*, 2023. 5
- [9] Ben Fei, Zhaoyang Lyu, Liang Pan, Junzhe Zhang, Weidong Yang, Tianyue Luo, Bo Zhang, and Bo Dai. Generative diffusion prior for unified image restoration and enhancement. In *CVPR*, pages 9935–9946. IEEE, 2023. 1, 2, 3, 4, 7, 8
- [10] Chunle Guo, Chongyi Li, Jichang Guo, Chen Change Loy, Junhui Hou, Sam Kwong, and Runmin Cong. Zero-reference deep curve estimation for low-light image enhancement. In *CVPR*, pages 1777–1786. Computer Vision Foundation / IEEE, 2020. 4
- [11] Chunle Guo Guo, Chongyi Li, Jichang Guo, Chen Change Loy, Junhui Hou, Sam Kwong, and Runmin Cong. Zero-reference deep curve estimation for low-light image enhancement. In *Proceedings of the IEEE conference on computer vision and pattern recognition (CVPR)*, pages 1780–1789, 2020. 7, 8
- [12] Xiaojie Guo, Yu Li, and Haibin Ling. Lime: Low-light image enhancement via illumination map estimation. *IEEE Transactions on Image Processing*, 26(2):982–993, 2017. 7
- [13] X.J. Shi H.D. Cheng. A simple and effective histogram equalization approach to image enhancement. In *Digital Signal Processing*, 2004. 4
- [14] Amir Hertz, Ron Mokady, Jay Tenenbaum, Kfir Aberman, Yael Pritch, and Daniel Cohen-Or. Prompt-to-prompt image editing with cross attention control. In *International Conference on Learning Representations*, 2023. 5
- [15] Amir Hertz, Andrey Voynov, Shlomi Fruchter, and Daniel Cohen-Or. Style aligned image generation via shared attention. In *CVPR*, 2024. 6, 7
- [16] J. Ho, A. Jain, and P. Abbeel. Denoising diffusion probabilistic models. In *Advances in Neural Information Processing Systems*, pages 6840–6851, 2020. 4
- [17] Jinhui Hou, Zhiyu Zhu, Junhui Hou, Hui Liu, Huanqiang Zeng, and Hui Yuan. Global structure-aware diffusion process for low-light image enhancement. In *NeurIPS*, 2023. 7, 8
- [18] Jinhui Hou, Zhiyu Zhu, Junhui Hou, Hui Liu, Huanqiang Zeng, and Hui Yuan. Global structure-aware diffusion process for low-light image enhancement. In *NeurIPS*, 2023. 4
- [19] Edward J Hu, Yelong Shen, Phillip Wallis, Zeyuan Allen-Zhu, Yuanzhi Li, Shean Wang, Lu Wang, and Weizhu Chen. LoRA: Low-rank adaptation of large language models. In *International Conference on Learning Representations*, 2022. 3, 6
- [20] Xun Huang and Serge Belongie. Arbitrary style transfer in real-time with adaptive instance normalization. In *ICCV*, 2017. 3, 6
- [21] Hai Jiang, Ao Luo, Haoqiang Fan, Songchen Han, and Shuaicheng Liu. Low-light image enhancement with wavelet-based diffusion models. *ACM Trans. Graph.*, 42(6): 238:1–238:14, 2023. 4
- [22] Hai Jiang, Ao Luo, Xiaohong Liu, Songchen Han, and Shuaicheng Liu. Lightendiffusion: Unsupervised low-light image enhancement with latent-retinex diffusion models. In *European Conference on Computer Vision*, 2024. 4
- [23] Lei Zhang Jianrui Cai, Shuhang Gu. Learning a deep single image contrast enhancer from multi-exposure images. In *TIP*, 2018. 8
- [24] Yunji Kim, Jiyoung Lee, Jin-Hwa Kim, Jung-Woo Ha, and Jun-Yan Zhu. Dense text-to-image generation with attention modulation. In *ICCV*, 2023. 5, 6, 7
- [25] Chulwoo Lee, Chul Lee, and Chang-Su Kim. Contrast enhancement based on layered difference representation of 2d histograms. *IEEE Transactions on Image Processing*, 22(12):5372–5384, 2013. 7
- [26] Chongyi Li, Chunle Guo, Wenqi Ren, Runmin Cong, Junhui Hou, Sam Kwong, and Dacheng Tao. An underwater image enhancement benchmark dataset and beyond. In *IEEE Transactions on Image Processing*, 2019. 1
- [27] Guofa Li, Yifan Yang, Xingda Qu, Dongpu Cao, and Keqiang Li. A deep learning based image enhancement approach for autonomous driving at night. In *Knowledge-Based Systems*, 2021. 1
- [28] Zhixin Liang, Chongyi Li, Shangchen Zhou, Ruicheng Feng, and Chen Change Loy. Iterative prompt learning for unsupervised backlit image enhancement. In *ICCV*, 2023. 2
- [29] Orly Liba, Kiran Murthy, Yun-Ta Tsai, Tim Brooks, Tianfan Xue, Nikhil Karnad, Qirui He, Jonathan T. Barron, Dillon Sharlet, Ryan Geiss, Samuel W. Hasinoff, Yael Pritch, and Marc Levoy. Handheld mobile photography in very low light. In *ACM Transactions on Graphics (TOG)*, 2019. 1
- [30] Yuhao Liu, Zhanghan Ke, Fang Liu, Nanxuan Zhao, and Rynson W.H. Lau. Diff-plugin: Revitalizing details for diffusion-based low-level tasks. In *CVPR*, 2024. 4

- [31] Feifan Lv, Feng Lu, Jianhua Wu, and Chongsoon Lim. MBLLEN: low-light image/video enhancement using cnns. In *British Machine Vision Conference 2018, BMVC 2018, Newcastle, UK, September 3-6, 2018*, page 220. BMVA Press, 2018. 4
- [32] Xiaoqian Lv, Shengping Zhang, Chenyang Wang, Yichen Zheng, Bineng Zhong, Chongyi Li, and Liqiang Nie. Fourier priors-guided diffusion for zero-shot joint low-light enhancement and deblurring. In *Proceedings of the IEEE/CVF Conference on Computer Vision and Pattern Recognition*, pages 25378–25388, 2024. 5
- [33] Kede Ma, Kai Zeng, and Zhou Wang. Perceptual quality assessment for multi-exposure image fusion. *IEEE Transactions on Image Processing*, 24(11):3345–3356, 2015. 2, 7
- [34] Long Ma, Tengyu Ma, Risheng Liu, Xin Fan, and Zhongxuan Luo. Toward fast, flexible, and robust low-light image enhancement. In *Proceedings of the IEEE/CVF Conference on Computer Vision and Pattern Recognition*, pages 5637–5646, 2022. 7
- [35] Chenlin Meng, Yutong He, Yang Song, Jiaming Song, Jiajun Wu, Jun-Yan Zhu, and Stefano Ermon. Sdedit: Guided image synthesis and editing with stochastic differential equations. In *International Conference on Learning Representations*, 2021. 5
- [36] Anish Mittal, Rajiv Soundararajan, and Alan C. Bovik. Making a “completely blind” image quality analyzer. *IEEE Signal Processing Letters*, 20(3):209–212, 2013. 8
- [37] Kristina Monakhova, Stephan R. Richter, Laura Waller, and Vladlen Koltun. Dancing under the stars: Video denoising in starlight. In *Proceedings of the IEEE/CVF Conference on Computer Vision and Pattern Recognition (CVPR)*, pages 16241–16251, 2022. 4
- [38] Cindy M Nguyen, Eric R Chan, Alexander W Bergman, and Gordon Wetzstein. Diffusion in the dark: A diffusion model for low-light text recognition. In *Proceedings of the IEEE/CVF Winter Conference on Applications of Computer Vision*, 2024. 4
- [39] Stephen M. Pizer, E. Philip Amburn, John D. Austin, Robert Cromartie, Ari Geselowitz, Trey Greer, Bart Ter Haar Romeny, and John B. Zimmerman. Adaptive histogram equalization and its variations. *Comput. Vision Graph. Image Process.*, 39(3):355–368, 1987. 4
- [40] Tunai Porto Marques and Alexandra Branzan Albu. L2uwe: A framework for the efficient enhancement of low-light underwater images using local contrast and multi-scale fusion. In *Proceedings of the IEEE/CVF Conference on Computer Vision and Pattern Recognition Workshops*, 2020. 1
- [41] S. Rahman, M. M. Rahman, M. Abdullah-Al-Wadud, G. D. Al-Quaderi, and M. Shoyuib. An adaptive gamma correction for image enhancement. *EURASIP Journal on Image and Video Processing*, 2016(1):1–13, 2016. 4
- [42] Liu Risheng, Ma Long, Zhang Jiaao, Fan Xin, and Luo Zhongxuan. Retinex-inspired unrolling with cooperative prior architecture search for low-light image enhancement. In *Proceedings of the IEEE Conference on Computer Vision and Pattern Recognition*, 2021. 2, 7, 8
- [43] R. Rombach, A. Blattmann, D. Lorenz, P. Esser, and B. Ommer. High-resolution image synthesis with latent diffusion models. In *Proceedings of the IEEE/CVF Conference on Computer Vision and Pattern Recognition*, pages 10684–10695, 2022. 4
- [44] J. Sohl-Dickstein, E. Weiss, N. Maheswaranathan, and S. Ganguli. Deep unsupervised learning using nonequilibrium thermodynamics. In *International Conference on Machine Learning*, pages 2256–2265. PMLR, 2015. 4
- [45] Jiaming Song, Chenlin Meng, and Stefano Ermon. Denoising diffusion implicit models. In *International Conference on Learning Representations*, 2021. 5
- [46] Y. Song and S. Ermon. Generative modeling by estimating gradients of the data distribution. In *Advances in Neural Information Processing Systems*, 2019. 4
- [47] Y. Song, J. Sohl-Dickstein, D. P. Kingma, A. Kumar, S. Ermon, and B. Poole. Score-based generative modeling through stochastic differential equations. In *ICLR*, 2021. 4
- [48] Narek Tumanyan, Michal Geyer, Shai Bagon, and Tali Dekel. Plug-and-play diffusion features for text-driven image-to-image translation. In *Proceedings of the IEEE/CVF Conference on Computer Vision and Pattern Recognition (CVPR)*, pages 1921–1930, 2023. 3, 5, 6, 7
- [49] Shuhang Wang, Jin Zheng, Hai-Miao Hu, and Bo Li. Naturalness preserved enhancement algorithm for non-uniform illumination images. *IEEE Transactions on Image Processing*, 22(9):3538–3548, 2013. 2, 7
- [50] Yufei Wang, Yi Yu, Wenhan Yang, Lanqing Guo, Lap-Pui Chau, Alex C. Kot, and Bihan Wen. Exposediffusion: Learning to expose for low-light image enhancement. In *ICCV*, pages 12404–12414. IEEE, 2023. 4
- [51] Chen Wei, Wenjing Wang, Wenhan Yang, and Jiaying Liu. Deep retinex decomposition for low-light enhancement. In *British Machine Vision Conference 2018, BMVC 2018, Newcastle, UK, September 3-6, 2018*, page 155. BMVA Press, 2018. 2, 4, 7, 8, 12
- [52] Saining Xie and Zhuowen Tu. Holistically-nested edge detection. In *Proceedings of the IEEE international conference on computer vision*, pages 1395–1403. IEEE, 2015. 3, 5
- [53] Xiaogang Xu, Ruixing Wang, Chi-Wing Fu, and Jiaya Jia. Snr-aware low-light image enhancement. In *2022 IEEE/CVF Conference on Computer Vision and Pattern Recognition (CVPR)*, pages 17693–17703, 2022. 7, 8
- [54] Meifang Yang, Xin Nie, and Ryan Wen Liu. Coarse-to-fine luminance estimation for low-light image enhancement in maritime video surveillance. In *2019 IEEE Intelligent Transportation Systems Conference (ITSC)*, 2019. 1
- [55] Peiqing Yang, Shangchen Zhou, Qingyi Tao, and Chen Change Loy. PGDiff: Guiding diffusion models for versatile face restoration via partial guidance. In *NeurIPS*, 2023. 5
- [56] Wenhan Yang, Wenjing Wang, Haofeng Huang, Shiqi Wang, and Jiaying Liu. Sparse gradient regularized deep retinex network for robust low-light image enhancement. *IEEE Trans. Image Process.*, 30:2072–2086, 2021. 4, 7, 8, 9, 12
- [57] X. Yi, H. Xu, H. Zhang, L. Tang, and J. Ma. Diff-retinex: Rethinking low-light image enhancement with a generative diffusion model. In *ICCV*, 2023. 4

- [58] Jeffrey Zhang, Shao-Yu Chang, Kedan Li, and David Forsyth. Preserving image properties through initializations in diffusion models. In *Proceedings of the IEEE/CVF Winter Conference on Applications of Computer Vision*, pages 5242–5250, 2024. [5](#)
- [59] Lvmin Zhang, Anyi Rao, and Maneesh Agrawala. Adding conditional control to text-to-image diffusion models. In *ICCV*, 2023. [3](#), [5](#)
- [60] Richard Zhang, Phillip Isola, Alexei A. Efros, Eli Shechtman, and Oliver Wang. The unreasonable effectiveness of deep features as a perceptual metric. In *2018 IEEE/CVF Conference on Computer Vision and Pattern Recognition*, pages 586–595, 2018. [8](#)
- [61] Yonghua Zhang, Jiawan Zhang, and Xiaojie Guo. Kindling the darkness: A practical low-light image enhancer. In *Proceedings of the 27th ACM International Conference on Multimedia*, page 1632–1640, New York, NY, USA, 2019. Association for Computing Machinery. [7](#), [8](#)
- [62] Yonghua Zhang, Xiaojie Guo, Jiayi Ma, Wei Liu, and Jiawan Zhang. Beyond brightening low-light images. *Int. J. Comput. Vision*, 129(4):1013–1037, 2021. [7](#), [8](#)